

# Deep-level structure of the spin-active recombination center in dilute nitrides

A. C. Ulibarri,<sup>1,\*</sup> C. T. K. Lew,<sup>2</sup> S. Q. Lim,<sup>2</sup> J. C. McCallum,<sup>3</sup> B. C. Johnson,<sup>4</sup> J. C. Harmand,<sup>5</sup> J. Peretti,<sup>1</sup> and A. C. H. Rowe<sup>1,†</sup>

<sup>1</sup>*Laboratoire de physique de la matière condensée, CNRS, Ecole Polytechnique, IP Paris, 91128 Palaiseau, France*

<sup>2</sup>*Centre of Excellence for Quantum Computation and Communication Technology, School of Physics, University of Melbourne, Melbourne, VIC 3010, Australia*

<sup>3</sup>*School of Physics, University of Melbourne, Parkville, VIC, Australia*

<sup>4</sup>*CQC2T, School of Engineering, RMIT University, Melbourne 3001, Australia*

<sup>5</sup>*Centre de Nanosciences et de Nanotechnologies, CNRS, Université Paris-Saclay, 91120 Palaiseau, France*

(Dated: October 30, 2023)

A paramagnetic, Gallium interstitial defect ( $\text{Ga}_i$ ) is thought to be responsible for a spectacular effect known as spin-dependent recombination (SDR) in dilute nitride semiconductors of the form  $\text{GaAs}_{1-x}\text{N}_x$ . Based on the magnitude and excitation power dependence of the SDR, it is widely accepted that this defect results in two deep levels within the gap corresponding to the  $(+/0)$  and  $(++/+)$  charge-state transitions. Using a novel form of photo-induced current transient spectroscopy that exploits the optical selection rules for band-to-band absorption of circularly polarized light, the deep-level electronic structure of an alloy with  $x = 0.021$  is revealed. The  $(+/0)$  state lies  $\approx 0.27$  eV below the conduction band edge, and an anomalous, negative activation energy reveals the presence of not one but *two* other states within the gap. The experimental observations are consistent with a  $(++/+)$  state lying  $\approx 0.13$  eV above the valence band edge, and a hitherto ignored, acceptor-like  $(+++ / +++)$  state lying approximately within  $k_B T = 25$  meV of the valence band edge. These observations can inform future efforts to improve current models, both of the unusual spin-dependent charge dynamics occurring at these centers, and of the local chemical environment of the  $\text{Ga}_i$  defect.

Spin-dependent Shockley-Read-Hall recombination (SDR) occurs at a paramagnetic recombination center that couples the minority carrier charge dynamics to their spin via a dynamic polarization of the centers [1]. In order to observe SDR, conduction electrons must be spin-polarized, and this is most commonly achieved using large, static magnetic fields. On resonance in a radio-frequency field, the SDR is then revealed in a measurable quantity related to the charge dynamics, for example the photo-luminescence (PL) intensity [2] or the photo-current (PC) [3]. This is the basis for optically- and electrically-detected magnetic resonance (ODMR and EDMR respectively), methods that have become important in the context of spin-based quantum technologies [4].

When the band-to-band optical selection rules permit the optical orientation of non-equilibrium conduction electron spins [5], it is also possible to observe SDR in zero field [1, 6]. The effect is particularly striking in dilute nitrides of the form  $\text{GaAs}_{1-x}\text{N}_x$  where increases in PL intensities up to one order of magnitude are observed when passing from a linearly- to a circularly-polarized pump [6, 7]. ODMR indicates that the paramagnetic center responsible for the SDR in these materials is the Gallium interstitial,  $\text{Ga}_i$ , in the  $(++)$  charge state [8, 9], although the exact details of the local alloy disorder is unclear [10]. While there is therefore partial information

available on the crystallographic nature of the spin-active defect, nothing is known about its electronic structure despite the fact that this is fundamental to its characteristics as a mediator of extremely rapid SDR [7]. This absence is addressed here using a novel, light-polarization-dependent form of photo-induced current transient spectroscopy [11] (or pol-PICTS) that provides an alternative means to achieve spin sensitivity in a deep-level transient spectroscopy [12].

The alloy studied here is a p-type ( $p = 10^{18} \text{ cm}^{-3}$ ), 50 nm thick epilayer of  $\text{GaAs}_{1-x}\text{N}_x$  grown by molecular beam epitaxy onto a GaAs substrate [13]. When continuously photo-excited at a wavelength of 887 nm, PL spectra of the form shown in Fig. 1 are obtained. The SDR is apparent from the factor of 5 increase in the PL intensity when switching from a linearly-polarized pump ( $\pi$ , black spectrum) to a circularly-polarized pump ( $\sigma$ , red spectrum). The insets provide a schematic explanation of how SDR arises. The three states of the centre corresponding to the  $(+/0)$ ,  $(++/+)$ , and  $(+++ / +++)$  charge state transitions are shown lying in the gap between the conduction band edge,  $E_c$ , and the valence band edge,  $E_v$  [10]. In what follows the names and densities of these three states are labelled using a subscript corresponding to the electron occupation numbers,  $N_2$ ,  $N_1$ , and  $N_0$  respectively [14].

With a  $\pi$ -polarized pump the conduction electrons and valence holes are unpolarized and four capture processes are possible as shown in Fig. 1 (black inset); electron capture on  $N_1$  at rate  $c_{n1}$  to form  $N_2$ , electron capture on  $N_0$  at rate  $c_{n0}$  to form  $N_1$ , hole capture on  $N_1$  at

\* agathaulibarri@yahoo.com

† alistair.rowe@polytechnique.edu

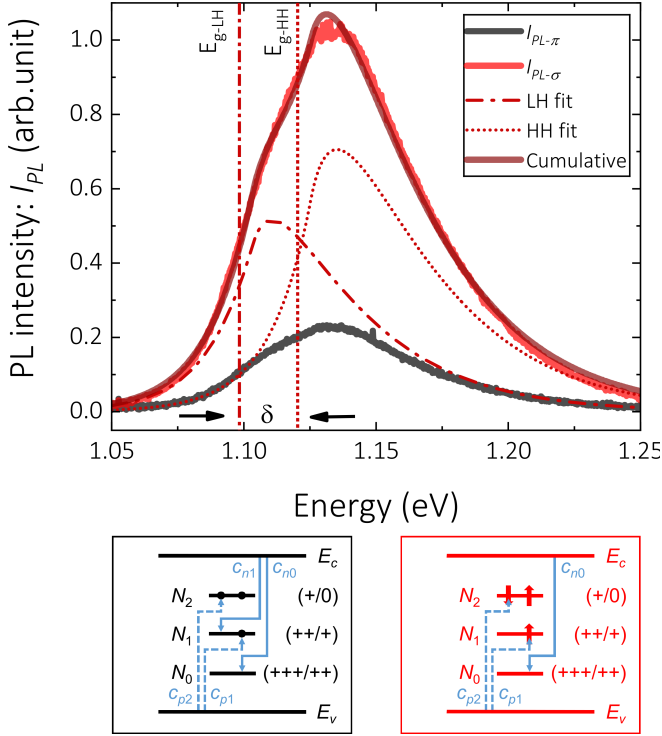


FIG. 1. Room-temperature PL spectra of  $\text{GaAs}_{0.979}\text{N}_{0.021}$ . Spectra are shown for a  $\pi$ -polarized pump in black, and a  $\sigma$ -polarized pump in red. The dramatic increase in PL intensity under a  $\sigma$ -pump is due to SDR [6]. The insets show the allowed capture processes (electrons with solid lines, holes with dotted lines) under the two pump polarizations. The minimum energy gap determined from the spectrum is  $E_{g\text{-LH}} = 1.09$  eV.

rate  $c_{p1}$  to form  $N_0$ , and hole capture on  $N_2$  at rate  $c_{p2}$  to form  $N_1$ . If the  $\sigma$ -polarized pump results in a 100 % spin polarized conduction electron population, the paramagnetic  $N_1$  states become 100 % polarized dynamically [1, 6, 14]. The exchange interaction on the centre then forbids electron capture to  $N_1$  [15] as indicated in Fig. 1 (red inset). Note that if the conduction electrons are not fully polarized this process is merely suppressed. Its suppression or absence increases the conduction electron lifetime yielding the observed increase in PL intensity. For the SDR to be large as observed, either  $c_{n1} \gg c_{n0}$  or the  $N_0$  state should be absent. The first condition is related to a difference in capture cross sections as discussed below. However, it is the latter approximation which is generally assumed in the literature [14].

Of importance here is the estimation of the gap of the alloy from the shape of the spectrum as described in detail elsewhere [16]. A two Roosbroeck-Shockley component fit to the red spectrum in Fig. 1 reveals that the heavy holes (red, dotted fit) and light holes (red, dash-dot fit) have different gaps labeled  $E_{g\text{-LH}} = 1.09$  eV and  $E_{g\text{-HH}} = 1.12$  eV respectively. The splitting between the two,  $\delta = 30$  meV, corresponds to an alloy containing 2.1 % nitrogen i.e.  $x = 0.021$ . The minimum gap of the

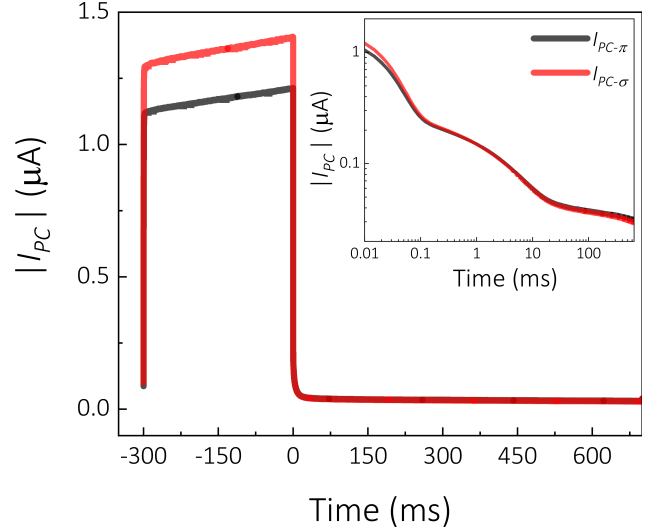


FIG. 2. Typical PICTS sequence with either a  $\sigma$ -polarized (red) or a  $\pi$ -polarized (black) filling pulse. The filling pulse is 300 ms long and the SDR appears as an increase in the PC measured under a  $\sigma$ -polarized pump. The PC transients measured over 700 ms after the filling pulse show non-exponential behavior (inset).

$\text{GaAs}_{0.979}\text{N}_{0.021}$  is thus  $E_{g\text{-LH}}$  which will be used below.

The  $\text{GaAs}_{0.979}\text{N}_{0.021}$  is electrically contacted with two micro-bonded aluminum wires separated by approximately  $170 \mu\text{m}$  which facilitates measurement of a photocurrent when the 887 nm pump is focused to a  $\approx 6 \mu\text{m}$  spot between the contacts, and when a voltage of  $-7$  V is applied. The SDR displays a characteristic peaked power dependence [14], and it is found that maximum SDR is achieved here for a 35 mW pump. This pump power and applied voltage is used throughout (see Supplementary Material).

In a PICTS measurement, the photo-excitation amplitude is modulated in time. Here the so-called filling pulse during which the sample is optically pumped is 300 ms long and the following dark period, achieved using a fast electro-optic modulator as a switch, is 700 ms long. It is during this dark period that the PC transient is measured at a 200 kHz sampling rate. A typical time trace of the photo current is shown in Fig. 2.

During the filling pulse a larger absolute PC,  $\|I_{PC}\|$ , is measured when using a  $\sigma$ -polarized pump due to SDR. The increase is smaller than that recorded in the PL spectra of Fig. 1 because the drift time of photo-carriers to the contacts is large compared to the minority carrier lifetime. Spin relaxation during transport then reduces the conduction electron spin-polarization and therefore the SDR [17]. The other important point is that during the return-to-equilibrium following the filling pulse, the PC transient is not a single exponential as seen in the log-log plot shown inset in Fig. 2. This is the usual case in a semiconductor and requires specific analysis methods to extract the exponential components, notably the tra-

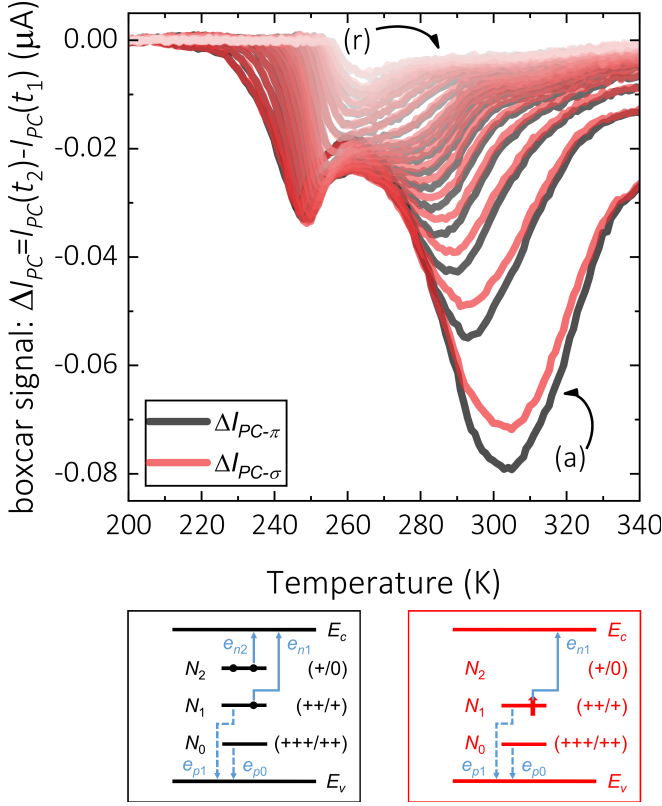


FIG. 3. The boxcar signal obtained with a  $\pi$ -polarized (black) and  $\sigma$ -polarized filling pulse (red). Two peaks are clear to the eye. The amplitude of the higher temperature of the two is polarization-dependent and is associated with electron emission from the  $N_2$  state (see text). The lower temperature of the two is independent of polarization and exhibits an anomalous shift to higher temperature as the rate window is shifted to lower rates. The insets show the allowed emission processes following a  $\pi$ -polarized filling pulse (in black), and a  $\sigma$ -polarized filling pulse resulting in 100 % spin-polarized conduction electrons.

ditional boxcar method [11] or the more modern inverse Laplace transform method [18].

An application of the boxcar method to the polarization-dependent PC transients measured over a temperature range of  $200 \text{ K} < T < 340 \text{ K}$  is shown in Fig. 3. The boxcar signals,  $\Delta I_{PC}$ , corresponding to a selection of rate windows ranging from  $\{t_1, t_2\} = \{1 \text{ ms}, 3 \text{ ms}\}$  labeled (a) in Fig. 3, to  $\{36 \text{ ms}, 108 \text{ ms}\}$  labeled (r) in Fig. 3. These two limiting cases define a rate window range shown in gray on the left in Fig. 5, with the maximum rate (a) equal to  $1220 \text{ s}^{-1}$ , and the minimum rate (r) equal to  $34 \text{ s}^{-1}$ . The full list of rate windows corresponding to the curves in Fig. 3 are given in the Supplementary Material. The signals obtained with a  $\sigma$ -polarized ( $\pi$ -polarized) filling pulse are shown in red (black). A three-component Gaussian fit to each curve (see Supplementary Material) reveals the possible presence of three peaks in temperature, two of which are clear to the eye in Fig. 3. The third peak does not appear in the inverse

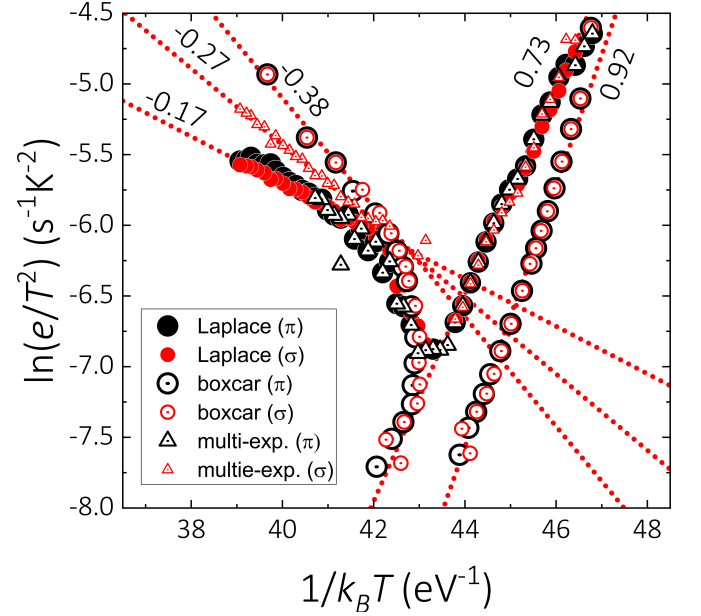


FIG. 4. Arrhenius plots generated from the boxcar (open, dotted circles), inverse Laplace transform (filled circles) and multi-exponential fit (open, dotted triangles) analyses. Colors correspond to filling pulse polarization. The slopes marked along the red, dotted fit lines correspond to activation energies when multiplied by -1.

Laplace transform analysis and will be ignored in what follows. The lower temperature peak's amplitude does not depend on the filling pulse polarization, and its position shifts anomalously to higher temperatures as the rate window is shifted to lower rates i.e. rate window (a) to rate window (r). The higher temperature peak's amplitude *does* depend on filling pulse polarization, with a lower amplitude measured for the  $\sigma$ -polarized filling pulse. Its position shifts to low temperatures as the rate window is shifted to lower rates as would be expected for a normal, thermally-activated process. The higher temperature, polarization-dependent peak will be analyzed first.

The polarization-dependent capture processes occurring during the filling pulse of the pol-PICTS measurement are those shown (inset) in Fig. 1. In the case of a  $\pi$ -polarized filling pulse and after an initial (immeasurably) fast recombination of conduction band electrons to the valence band, the conduction band electron population changes on the timescales of the experimental rate window range (1 ms to 108 ms) due to charge re-emission from deep levels according to:

$$\frac{dn}{dt} = e_{n2}N_2 + e_{n1}N_1, \quad (1)$$

where  $e_{n2}$  and  $e_{n1}$  are the electron emission rates from the  $N_2$  and  $N_1$  states respectively as shown in the insets of Fig. 3. The valence band hole population changes

according to:

$$\frac{dp}{dt} = e_{p1}N_1 + e_{p0}N_0, \quad (2)$$

where  $e_{p1}$  and  $e_{p0}$  are the hole emission rates from the  $N_1$  and  $N_0$  states respectively, also shown inset in Fig. 3. The overall PC transient like those shown in Fig. 2 results from a sum of Eq. (1) and Eq. (2), weighted for the transport coefficients.

In the case of the  $\sigma$ -polarized filling pulse, and in the limit of a 100 % spin-polarized conduction electron population, electron capture to the  $N_1$  is no longer allowed as explained above and indicated in Fig. 1 (red inset). In this case there is no capture process which produces centers in the  $N_2$  state and the first term in Eq. (1) is absent as shown schematically in Fig. 3 (red inset). The resulting reduction in the amplitude of the PC transient manifests itself as a reduction in the boxcar amplitude. Note again that if the conduction electron spin-polarization is lower than 100 %, the boxcar amplitude is reduced but is not zero. It is thus straightforward to associate the polarization-dependent boxcar peak, whose amplitude decreases when switching to the  $\sigma$ -polarized filling pulse, with electron emission from the  $N_2$  states at rate  $e_{n2}$ . Note that only the change in amplitude with filling pulse polarization is accounted for here. The absolute change in amplitude of both the red and black curves in Fig. 3 with a change in rate window arises because of transport effects, but this does not affect the determination of activation energies [11].

Using the usual rate-window procedure to associate the temperature of the boxcar peak with an emission rate, an Arrhenius plot like that shown in Fig. 4 can be constructed. In a thermally activated process of the form

$$e_{n2}(T) = e_{n2}^0 \exp[-E_{n2}/k_B T], \quad (3)$$

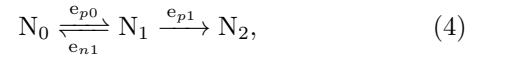
the slope of the Arrhenius plot associated with the  $e_{n2}$  emission process yields an activation energy of 0.38 eV, taken from the high temperature points where the peak in Fig. 3 is most visible (for a  $\pi$ -polarized filling pulse this is shown by the open, dotted, black circles in Fig. 4(a)). The activation energy itself does not depend on the polarization of the filling pulse (the  $\sigma$ -polarization case is indicated by open, red, dotted circles in Fig. 4). This result is checked using the inverse Laplace transform method [18] which yields a slightly different activation energy of 0.17 eV (filled, red and black circles in Fig. 4(b)). Finally, a reality check with a  $n$ -component exponential fit to the transients, where  $n$  is determined during the regularization part of the Laplace transform procedure, yields an activation energy of 0.27 eV. Taking the average of these three results yields an estimation,  $E_{n2} = 0.27$  eV, which is associated with the  $N_2$  state lying 0.27 eV below the conduction band edge as shown on the right in Fig. 5 [19].

We now turn to the analysis of the lower temperature boxcar peak in Fig. 3 whose amplitude is independent of polarization, and which exhibits an anomalous shift to

higher temperatures at slower rate windows. On the boxcar Arrhenius plot in Fig. 4 this appears as an activated process with an anomalous, negative activation energy of -0.92 eV (open, dotted circles) which is independent of filling pulse polarization. The inverse Laplace transform analysis shows the presence of this emission process with an anomalous activation energy of -0.73 eV (filled circles), as does the multi-exponential fit (open, dotted triangles). The average of these three results yields an effective activation energy,  $E_{\text{eff}} = -0.8$  eV.

At first sight a negative activation energy is puzzling, but in fact this situation is encountered in a number of interesting situations in chemistry. Examples include the oxidation of nitrous oxide [20], the cracking of n-paraffins [21], and cell death rates as a result of hypothermia [22]. In each of these cases, the negative activation energy is explained by a multi-step process consisting of a fast, reversible reaction between the reactants and an intermediate product, which then proceeds via a slow, irreversible process to the final products. The essential idea is that the intermediate state must have a large activation energy so that it is preferentially emptied as temperature rises, thereby cutting off the route to the formation of the final products whose concentration will then *decrease* with increasing temperature. An excellent generic description of this is given in Ref. 22.

Inspired by this, a similar configuration is proposed here, starting with a fast, reversible exchange between  $N_1$  and  $N_0$  states, followed by a slow conversion of  $N_1$  states to  $N_2$  states via hole emission according to:



where, importantly, each of the emission rates appearing in the reaction and sketched in Fig. 3 (insets) are normally activated i.e.

$$\begin{aligned} e_{n1}(T) &= e_{n1}^0 \exp[-E_{n1}/k_B T] \\ e_{p0}(T) &= e_{p0}^0 \exp[-E_{p0}/k_B T] \\ e_{p1}(T) &= e_{p1}^0 \exp[-E_{p1}/k_B T], \end{aligned} \quad (5)$$

with  $E_{n1}$ ,  $E_{p0}$ , and  $E_{p1}$  all *positive*. To obtain an effective negative activation energy in the following, the condition

$$e_{p1} \ll e_{p0}, e_{n1} \quad (6)$$

in Eq. (4) should be fulfilled [22]. Note that unlike the general assumption made throughout the literature that  $N_0$  states are absent [14], the observation of a negative effective activation energy *requires* the presence of  $N_0$  states.

Ab-initio calculations of the electronic structure of Ga<sub>i</sub> in both GaAs [23] and GaAsN [10] suggest that the  $N_0$  state lies close to the valence band edge. We therefore postulate that the activation energy for the hole emission at rate  $e_{p0}$  is within  $k_B T \approx 25$  meV of the valence band edge i.e.  $E_{p0} = 0.025$  eV. This is the *only* energy in the electronic structure of the SDR-active center that

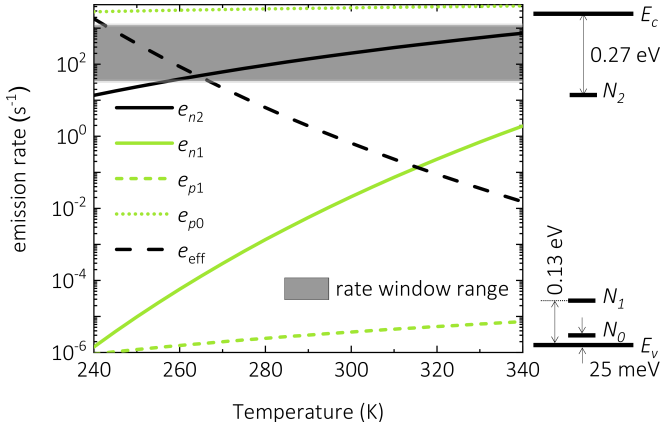


FIG. 5. Temperature variation of the emission rates given in Eq. (3) and Eq. (5) using the estimated activation energies. The rates  $e_{n2}$  and  $e_{\text{eff}}$  appearing in the rate window range (gray zone) that are measured in the experiment are shown in black. The negative slope of  $e_{\text{eff}}$  corresponds to an effective negative activation energy. The other rates, in green, fall outside the rate window range and are not directly measured in the experiment. To the right a schematic representation of the electronic structure of the  $\text{Ga}_i$  center is shown.

is not determined from the pol-PICTS experiment, and suggests that  $N_0$  is a shallow acceptor rather than a deep center. Its equilibrium density at room temperature is required to be small compared to the total  $\text{Ga}_i$  density for large SDR [14], and this is ensured by taking the rate amplitude  $e_{p0}^0$  in Eq. (5) to be sufficiently large compared to the other rate amplitudes. In the following a value of  $e_{p0}^0 = 10^4 \text{ s}^{-1}$  is used which, as seen by the green, dotted line in Fig. 5, does indeed make  $e_{p0}$  large compared to all other emission rates. Two important observations should be immediately noted in Fig. 5. Firstly, since  $N_0$  is shallow,  $e_{p0}$  only weakly depends on temperature, and secondly it falls outside the experimental rate window indicated in gray, meaning that  $e_{p0}$  is too fast to be directly measured in the experiment.

Unlike  $e_{p0}$ , the emission rate  $e_{n2}$  is directly measured in the experiment as already discussed. Since its activation energy,  $E_{n2} = 0.27 \text{ eV}$ , is already determined, a rate amplitude  $e_{n2}^0 = 10^7 \text{ s}^{-1}$  can be chosen so that  $e_{n2}$  does fall in the rate window range (see black line in Fig. 5). It is the only emission rate to do so for temperatures above 265 K as observed experimentally in Fig. 3. As the temperature drops below 265 K,  $e_{n2}$  slows noticeably since  $E_{n2}$  is relatively large, and approaches the edge of the experimental rate window. Once it passes out of the rate window it is too slow to be experimentally measurable. In this limit, the measurable rate of change of the photo-current transient due to electron emission into the conduction band in Eq. (1) becomes:

$$\frac{dn}{dt} \approx e_{n1}N_1. \quad (7)$$

Fig. 5 is obtained with rate amplitudes  $e_{n1}^0 = 10^{15} \text{ s}^{-1}$  and  $e_{p1}^0 = 10^{-3} \text{ s}^{-1}$ . We emphasize that the values

of the emission rate amplitudes are related to capture cross sections and can therefore vary over many orders of magnitude. However, their absolute values are not to be over-interpreted. Their relative values are however of interest. For example, the choice of  $e_{n1}^0$  and  $e_{p1}^0$  ensures the validity of Eq. (6) as seen by the relative positions of the three green lines in Fig. 5, and the choice of  $e_{n2}^0$  relative to  $e_{n1}^0$ , ensures that electron capture rates to  $N_1$  are greater than those to  $N_0$  i.e.  $c_{n1} \gg c_{n0}$  which ensures large SDR as mentioned in the introduction. The choice of amplitudes also ensures that a steady-state between the  $N_0$  and  $N_1$  concentrations is established on timescales much shorter than those required for the final step i.e. the conversion of  $N_1$  states to  $N_2$  states via hole emission at rate  $e_{p1}$ . This steady state is expressed as  $e_{p0}N_0 = e_{n1}N_1$  such that the electron and hole contributions to the PC transient from Eq. (7) and Eq. (2) can be written:

$$\frac{dn}{dt} \approx e_{p0}N_0 \quad (8)$$

and

$$\frac{dp}{dt} = \frac{e_{p0}e_{p1}}{e_{n1}}N_0 + e_{p0}N_0. \quad (9)$$

Since  $e_{p0}$  is outside the rate window range, the PC transient due to electron re-emission into the conduction band described by Eq. (8) is immeasurably fast. This is also true for the second term in Eq. (9) which is part of the hole contribution to the PC transient. The anomalous peak in the boxcar signal occurring below 265 K in Fig. 3 is therefore attributed to the first term in Eq. (9). Using Eq. (5),  $e_{\text{eff}} = e_{p0}e_{p1}/e_{n1}$  has an effective activation energy

$$E_{\text{eff}} = E_{p0} + E_{p1} - E_{n1} \quad (10)$$

which is *negative* if  $E_{n1} > E_{p0} + E_{p1}$ . With the measured, anomalous activation energy of  $E_{\text{eff}} = -0.8 \text{ eV}$  and  $E_{p0} = 0.025 \text{ eV}$  as previously stated, Eq. (10) yields  $E_{p1} - E_{n1} = -0.825 \text{ eV}$ . Combining this with knowledge of the gap from the PL spectrum in Fig. 1,  $E_{p1} + E_{n1} = 1.09 \text{ eV}$ , yields  $E_{n1} = 0.97 \text{ eV}$  and  $E_{p1} = 0.13 \text{ eV}$ . This result is sketched in the electronic structure in Fig. 5.

Fig. 5 shows the temperature dependence of  $e_{\text{eff}}$  (black, dashed line) which exhibits the expected negative slope corresponding to a negative activation energy, and moreover, which crosses the rate window range in the temperature range below 265 K where the anomalous peak in Fig. 3 appears. The figure is extremely useful to help physically summarize the observation of a negative activation energy. Consider a temperature rise from 240 K. On the scale of the changes in the emission rates with temperature  $e_{p0}$  is essentially constant because of its small activation energy. The generation of centres in the  $N_1$  state via this process is therefore essentially independent of temperature. On the other hand, electron emission at rate  $e_{n1}$  from  $N_1$  states to form  $N_0$  states increases

very significantly with temperature because of its large activation energy. Consequently, the rapid steady-state between  $N_0$  and  $N_1$  shifts towards an increase (decrease) in the density of  $N_0$  ( $N_1$ ) states. Note also that the repopulation of  $N_1$  states via electron emission from the  $N_2$  states cannot compensate for this since  $e_{n2}$  is less sensitive to temperature than  $e_{n1}$ . Increasing temperature therefore *depopulates* the  $N_1$  states.

Return now to the first term on the right hand side in Eq. (2). If the depopulation of  $N_1$  with increasing temperature is faster than the thermally activated increase in  $e_{p1}$ , then this term becomes smaller with increasing temperature. Since it is the only term in the rate window range below 265 K, the measured emission rate in the PC transient proportional to  $dp/dt$  will decrease anomalously with temperature resulting in an apparent negative activation energy. To paraphrase from Ref. 21 “This phenomenon is contrary to normal expectations, and is a consequence of the competition between two effects: the increase of intrinsic kinetics with temperature (here  $e_{p1}$ ), and the decrease of ... the concentration of active intermediates with temperature (here  $N_1$ ).”

In conclusion, using a novel pol-PICTS approach that adds spin-sensitivity to the usual PICTS method, the electronic structure of the paramagnetic center responsi-

ble for the spectacular SDR observed in dilute nitrides has been estimated for the first time. The result, shown sketched in Fig. 5, is as important as the crystallographic identification of the  $\text{Ga}_i$  center [8] in that the electronic structure fundamentally determines the nature of the electronic states as donors, acceptors, traps, or recombination centers. The observations are consistent with the presence of a shallow, acceptor-like state ( $N_0$ ) which has hitherto been ignored in coupled spin/charge models. Since these models only approximately reproduce the SDR properties of these alloys, the result can inform improvements to these models. The state energies are only in approximative agreement with ab initio calculations of the electronic structure that assume particular arrangements of nitrogen atoms around the  $\text{Ga}_i$  interstitial [10]. This should inspire new attempts to identify the local chemical environment of the SDR-active interstitial.

## ACKNOWLEDGMENTS

ACU acknowledges support of the FASIC program for travel support (*partenariat Hubert Curien franco-australien*). The authors thank N. Vast and Y. Cho for useful discussions.

- 
- [1] C. Weisbuch and G. Lampel, Solid-state Communications **14**, 141 (1974).
  - [2] S. Geschwind, R. J. Collins, and A. L. Schawlow, Physical Review Letters **3**, 545 (1959).
  - [3] D. J. Lepine, Physical Review B **6**, 436 (1972).
  - [4] D. D. Awschalom, R. Hanson, J. Wrachtrup, and B. B. Zhou, Nature Photonics **12**, 516 (2018).
  - [5] F. Meier and B. P. Zakharchenya, eds., *Optical orientation (Modern problems in condensed matter sciences vol. 8)* (Elsevier, 1984).
  - [6] V. K. Kalevich, E. L. Ivchenko, M. M. Afanasiev, A. Y. Shiryaev, A. Y. Egorov, V. M. Ustinov, B. Pal, and Y. Masumoto, Journal of Experimental and Theoretical Physics Letters **82**, 455 (2005).
  - [7] V. K. Kalevich, A. Y. Shiryaev, E. L. Ivchenko, A. Y. Egorov, L. Lombez, D. Lagarde, X. Marie, and T. Amand, JETP Letters **85**, 174 (2007).
  - [8] W. X. J., I. A. Buyanova, F. Zhao, D. Lagarde, A. Balocchi, X. Marie, C. Tu, J. C. Harmand, and W. M. Chen, Nature Materials **8**, 198 (2009).
  - [9] X. J. Wang, Y. Puttison, C. W. Tu, A. J. Ptak, V. K. Kalevich, A. Y. Egorov, L. Geelhaar, H. Riechert, W. M. Chen, and I. A. Buyanova, Applied Physics Letters **95**, 241904.
  - [10] P. Laukkanen, M. P. J. Punkkinen, J. Puustinen, H. Levämäki, M. Tuominen, K. Schulte, J. Dahl, J. Lång, H. L. Zhang, M. Kuzmin, K. Palotas, B. Johansson, M. Vitos, M. Guina, and K. Kokko, Physical Review B **86**, 195205 (2012).
  - [11] J. C. Baland, J. P. Zielinger, C. Noguét, and M. Tapiero, Journal of Physics D: Applied Physics **19**, 57 (1986).
  - [12] K. J. Myers, P. M. Lenahan, J. P. Ashton, and J. T. Ryan, Journal of Applied Physics **132**, 115301 (2022).
  - [13] J. C. Harmand, A. Caliman, E. V. K. Rao, L. Largeau, J. Ramos, R. Teissier, L. Travers, G. Ungaro, B. Theyss, and I. F. L. Dias, Semiconductor Science & Technology **17**, 778 (2002).
  - [14] E. L. Ivchenko, V. K. Kalevich, A. Y. Shiryaev, M. M. Afanasiev, and Y. Masumoto, Journal of Physics: Condensed Matter **22**, 465804 (2010).
  - [15] D. Kaplan, I. Solomon, and N. F. Mott, Journal de physique lettres **39**, 51 (1978).
  - [16] A. C. Ulibarri, R. Kothari, A. Garcia, J.-C. Harmand, S. Park, F. Cadiz, Y. Lassailly, J. Peretti, and A. C. H. Rowe, Physica Status Solidi (b) **260**, 2200361 (2023).
  - [17] A. Kunold, A. Balocchi, F. Zhao, T. Amand, N. B. Abdallah, J. C. Harmand, and X. Marie, Physical Review B **83**, 165202 (2011).
  - [18] J. H. Evans-Freeman, A. R. Peaker, I. D. Hawkins, P. Y. Y. Kan, J. Terry, L. Rubaldo, M. Ahmed, S. Watts, and L. Dobaczewski, Materials science in semiconductor processing **3**, 237 (2000).
  - [19] G. F. Neumark and K. Kosai, *Semiconductors and Semimetals vol. 19 Deep Levels, GaAs, Alloys, Photochemistry*, edited by R. K. Willardson and A. C. Beer, Vol. 19 (Academic Press, 1983).
  - [20] M. L. McKee, Journal of the American Chemical Society **117**, 1629 (1995).
  - [21] J. Wei, Chemical engineering science **51**, 2995 (1996).
  - [22] J. L. Muench, J. Kruuv, and J. R. Lepock, Cryobiology **33**, 253 (1996).
  - [23] G. A. Baraff and M. Schlüter, Physical Review Letters **55**, 1327 (1985).